2015 IEEE/RSJ International Conference on Intelligent Robots and Systems (IROS)
Congress Center Hamburg
Sept 28 - Oct 2, 2015. Hamburg, Germany

A Robot Self-Localization System using One-Way Ultra-Wideband Communication

Anton Ledergerber, Michael Hamer and Raffaello D'Andrea

***Abstract*— A robot localization system is presented that enables a robot to estimate its position within some space by passively receiving ultra-wideband radio signals from fixed-position modules. Communication from the fixed-position modules is one-way, allowing the system to scale to multiple robots. Furthermore, the system's high position update rate makes it suitable to be used in a feedback control system, and enables the robot to track and perform high-speed, dynamic motions.**

This paper describes the algorithmic underpinnings of the system, discusses design decisions and their impact on the performance of the resulting localization, and highlights challenges faced during implementation. Performance of the localization system is experimentally verified through comparison with data from a motion-capture system. Finally, the system's application to robot self-localization is demonstrated through integration with a quadrocopter.

I. Introduction

Several systems for robot localization currently exist. These are often based on acoustic, optical or radio measurements and vary in cost, accuracy and update frequency. Global Navigation Satellite Systems, for example the Global Positioning System (GPS) [1], and on-board SLAM algorithms [2] offer decentralized navigation, in which each robot is capable of localizing itself (self-localizing) within some environment. Off-board systems, such as motion-capture systems [3] or ultra-wideband localization (UWB) systems [4], may also be used for localization and allow the robot's position to be computed centrally by collecting measurements from a set of wired sensors.

This paper presents a localization system that enables a robot to self-localize based on the reception of UWB radio signals from fixed-position, wirelessly-connected modules (hereinafter referred as anchors). These anchors are placed at known locations, and periodically transmit UWB signals. By passively receiving these signals and recording their arrival times, the robot is able to self-localize relative to the anchors by using either time-of-arrival (TOA) or time-difference-of-arrival (TDOA) measurements. The system layout is illustrated in Fig. 1, and shares many architectural similarities to GNSS systems (e.g. GPS).

Since the robot is not active in the communication process and is able to self-localize, its position is not centrally tracked and anonymous operation is enabled. Furthermore, since the robot localizes itself passively, the system allows multiple robots to operate simultaneously within the space, without affecting the update rate of the system. This is in contrast to systems such as [5] and [6], which show how UWB measurements can be fused in an estimator, but wherein the robot plays an active role in the communication.

Our intention is that this paper serves as a basis for others interested in constructing such a localization system. To this effect, this paper will outline and summarize the theoretical underpinnings of the system and discuss algorithmic and implementation challenges. This paper is therefore structured as follows: In Section II, two schemes for localization, TOA and TDOA, are compared and contrasted in the context of robot self-localization. In Section III, the algorithmic underpinnings of the system are presented and challenges relating to the synchronization of anchor clocks are presented and addressed. The performance of the system is quantified in Section IV through comparison with motion-capture data. Finally, in Section V, the system's applicability to robot self-localization is demonstrated through integration with a quadrocopter system, enabling the quadrocopter to fly stable, repeatable and dynamic trajectories.

II. Methods of Robot Localization

Existing results, for example in [6], [7], demonstrate that a robot can use two-way communication with a set of anchors in order to self-localize. As presented in [8], it is also possible for a robot to be localized using one-way communication. However in these cases, the robot transmits a signal, which is received by a set of fixed-position receivers. By comparing reception times of each receiver, it is possible to compute

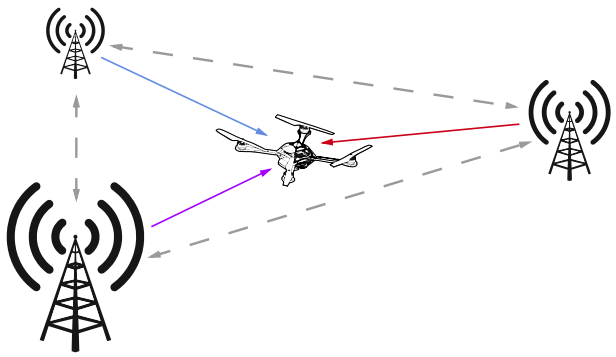

Fig. 1. The architecture of the localization system presented in this paper is shown in this figure. A robot receives UWB radio signals from fixed-position anchors. These anchors periodically transmit UWB signals which are recorded by the robot and used to localize itself relative to the anchors. Since the robot is not active in the communication process, the system allows multiple robots to operate simultaneously and anonymously within the space.

The authors are with the Institute for Dynamic Systems and Control, ETH Zurich, Switzerland {antonl,hamerm,rdandrea}@ethz.ch.

This research was supported by the NCCR Digital Fabrication, funded by the Swiss National Science Foundation. (NCCR Digital Fabrication Agreement #51NF40-141853)

the robot's location centrally using TDOA measurements. Such an architecture is often used for asset tracking [9], [10], where it is desirable to know the location of each asset centrally. This architecture was also employed in [11] to centrally track and control a swarm of lightweight robots, each with limited computational power.

In contrast to the research discussed above, the localization system presented in this paper has an architecture similar to GPS (refer Fig. 1), whereby a set of fixed-position anchors transmit signals that are received by robots within the space. By comparing the arrival time of each signal, a robot is able to self-localize. Since the robot is not active in this communication and is able to self-localize based on the received measurements, the system scales to support multiple robots simultaneously and anonymously utilizing the space.

Two different methods of localization – TOA and TDOA – are supported by the presented system, and are compared in the remainder of this section.

A. Time Difference of Arrival vs Time of Arrival

Localization algorithms based on signal propagation time can be categorized into those which use the arrival time of each signal (TOA algorithms), and those which use the difference between the arrival times of signals (TDOA algorithms).

A TOA measurement f_i is related to the position $\mathbf{p}$ of the robot and the position $\mathbf{p_i}$ of the transmitting anchor i by:

$$f_i = \frac{\|\mathbf{p}-\mathbf{p_i}\|}{c} - \Theta + n_i \tag{1}$$

$$= h_i(\mathbf{p}, \Theta, n_i) \tag{2}$$

where c is the speed of light, Θ is the robot's clock offset and n_i is the measurement and transmission noise. Note that, since TOA algorithms calculate time of flight (and hence distance) using the arrival time at the robot and the transmission time from the anchor, the robot's clock must be synchronized to the anchor's clock.

On the other hand, a TDOA measurement $d_{i,j}$ between the robot and anchors i and j is given by

$$d_{i,j} = \frac{\|\mathbf{p}-\mathbf{p_i}\| - \|\mathbf{p}-\mathbf{p_j}\|}{c} + n_i - n_j. \tag{3}$$

Note that TDOA algorithms use the difference between the arrival times of two signals, and as such, the offset of the robot's clock is canceled. Therefore, the robot's clock does not need to be synchronized with the anchors' clocks. While this leads to a simpler implementation, care must be taken to correctly handle the correlated noise of different TDOA measurements.

As illustrated in Fig. 2, localization using TDOA measurements or TOA measurements with an unsynchronized clock, requires calculation of the intersection of hyperbola [12], a solution which is quite sensitive to measurement noise. However, in the case of TOA algorithms, if the robot's clock is synchronized to the anchors' clocks or if two-way communication is used to omit synchronization, localization

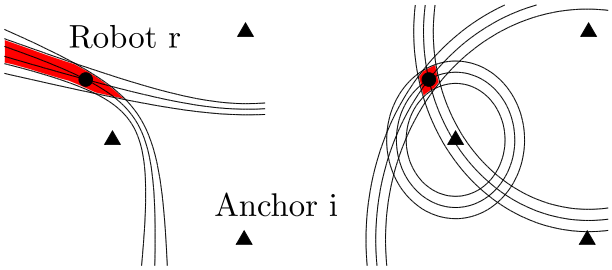

Fig. 2. Geometric solution sets for a given error tolerance. Left: TDOA and TOA localization with unsynchronized clocks. Right: TOA localization with a synchronized clock.

simplifies to calculating the intersection of spheres – a solution which is more robust to noise [12], [13]. The reduced sensitivity to noise afforded by clock synchronization is shown in the next section and, in particular, in Fig. 3.

B. Sensitivity of TOA and TDOA methods

In order to analyze the variance of the position estimate due to measurement noise for a two-dimensional setup, we linearize (2) around the state $\mathbf{x} = [\Theta, x, y]^T$ for a set of TOA measurements from N anchors. Assuming that the localization algorithm provides an unbiased estimate, the following first-order approximation between the deviations in its state estimate $\hat{\mathbf{x}}$ and the measurement and transmission noise $\mathbf{n} = [n_0, n_1, \ldots, n_{N-1}]^T$ can be made:

$$M(\hat{\mathbf{x}} - \mathbf{x}) = \mathbf{n}, \tag{4}$$

where

$$M = \frac{\partial [h_0, h_1, \ldots, h_{N-1}]^T}{\partial \mathbf{x}}. \tag{5}$$

If least squares is used to solve for the deviation of the state estimate, which is optimal in the case of Gaussian noise [14], the variance on the state estimate $\hat{\mathbf{x}}$ can be shown to be:

$$\mathrm{Var}(\hat{\mathbf{x}}) = \sigma_f^2 \left(M^T M\right)^{-1} \tag{6}$$

$$= \sigma_f^2 \left(\sum_{i=0}^{N-1} \left[\begin{array}{c|cc} 1 & \frac{\cos(\alpha_i)}{c} & \frac{\sin(\alpha_i)}{c} \\ \hline \frac{\cos(\alpha_i)}{c} & \frac{\cos^2(\alpha_i)}{c^2} & \frac{\sin(2\alpha_i)}{2c^2} \\ \frac{\sin(\alpha_i)}{c} & \frac{\sin(2\alpha_i)}{2c^2} & \frac{\sin^2(\alpha_i)}{c^2} \end{array} \right] \right)^{-1} \tag{7}$$

where σ_f^2 is the variance of the uncorrelated measurement noise, and α_i is the angle from anchor i to the robot, such that $\cos(\alpha_i) = (x_i - x)/\|\mathbf{p}-\mathbf{p_i}\|$ and $\sin(\alpha_i) = (y_i - y)/\|\mathbf{p}-\mathbf{p_i}\|$.

The covariance matrix (7) of the state estimate equals the Cramér-Rao Lower Bound (CRLB) for TOA measurements with an unknown clock offset and Gaussian measurement noise as calculated in [15]. The equivalence of the CRLB on the position for TDOA and TOA localization methods, under the assumption of an unknown clock offset, was shown in [16]. Further results from [15] suggest that both methods of localization have a similar computational complexity.

We take the approach of [15] and divide the inverted covariance matrix (7) into four sub-blocks, such that

$$\mathrm{Var}(\hat{\mathbf{x}}) = \begin{bmatrix} \mathrm{Var}(\hat{\Theta}) & \mathrm{Cov}(\hat{\Theta},\hat{\mathbf{p}}) \\ \mathrm{Cov}(\hat{\mathbf{p}},\hat{\Theta}) & \mathrm{Var}(\hat{\mathbf{p}}) \end{bmatrix} = \begin{bmatrix} J_\Theta & J_{\Theta,\mathbf{p}}^T \\ J_{\Theta,\mathbf{p}} & J_\mathbf{p} \end{bmatrix}^{-1}, \quad (8)$$

where J_Θ contains information of the clock-offset, $J_\mathbf{p}$ the position information and where $J_{\Theta,\mathbf{p}}$ are the cross-correlation terms.

If the variance on the position is calculated by a block-wise matrix inversion:

$$\mathrm{Var}(\hat{\mathbf{p}}) = \left(J_\mathbf{p} - J_{\Theta,\mathbf{p}} J_\Theta^{-1} J_{\Theta,\mathbf{p}}^T\right)^{-1}, \quad (9)$$

it is clearly visible how the uncertainty of the clock offset influences the variance of the position. Hence, under equal measurement noise, systems with synchronized clocks or systems which omit clock synchronization by using two-way communication are more accurate than one-way communication localization systems, since with perfect offset information ($J_\Theta \to \infty$) the position estimate variance is given as $\mathrm{Var}(\hat{\mathbf{p}}) = J_\mathbf{p}^{-1}$. Therefore, only in the case where $J_{\Theta,\mathbf{p}} = 0$ does the uncertainty of the clock offset not increase the variance of the position estimate. This is the case if the sensor configuration is first moment balanced ($\sum_{i=0}^{N-1}\cos(\alpha_i) = \sum_{i=0}^{N-1}\sin(\alpha_i) = 0$), i.e. if the anchors are distributed about the robot in an average sense; this is one criteria for optimal sensor placement as discussed in [17]. The variance for a setup with three anchors is shown in Fig. 3, where it is visible that a similar performance between one-way and two-way communication scheme can be achieved only inside the convex hull spanned by the anchors. However, this performance is equal for TDOA and for TOA with an unknown clock offset.

C. Dynamic Setup

If the robot is not stationary, but rather moving through the space, TOA systems with recursive clock and position offset estimation have a potential advantage in comparison to TDOA systems with only recursive position estimation. In the extreme case of a perfectly known clock model, the robot would only have to synchronize its clock once to the anchors' clocks, best at the position where $J_{\Theta,\mathbf{p}} = 0$ and over a large number of measurements sets M such that $J_\Theta = MN/\sigma_f^2$ becomes large. It could then rely on its clock model when moving through areas showing a poorer CRLB for the static scene and a similar performance to a two-way communication system could be achieved with a one-way communication system. Such a scenario is shown in Fig. 3 where the robot orbits one anchor. Starting with the azimuth angle $\phi = 0$ (placing the robot within the convex hull of the anchors, and hence in a region with low CRLB), it is able to initialize its estimator with accurate position and clock offset values. However, the worse the clock and its model, the less of an advantage it is to track the offset.

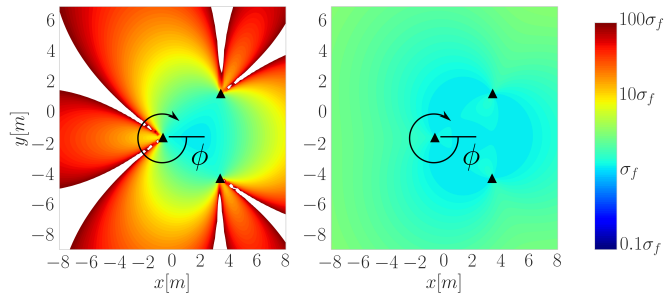

Fig. 3. The variance for an estimator using TDOA or TOA measurements with unknown clock offset (left) and for an estimator using TOA measurements with known clock offset (right). Both plots show $\sqrt{\mathrm{tr}(\mathrm{Var}(\hat{\mathbf{p}}))}$ for measurement noise with standard deviation σ_f.

III. Algorithm

Having compared TOA and TDOA algorithms in terms of their theoretical performance bounds (Fig. 3) and measurement equations in (1) and (3), we now present an algorithm that enables these measurements. We begin the development by discussing the clock model and requirement for synchronized anchor clocks, before presenting the algorithm in its entirety.

A. Clock Model

Using the terminology of [18], the local time of UWB module i (e.g. an anchor or robot) is denoted as $C_i(t)$, where $C_i(t) = t$ in the case of a perfect clock. However, since an imperfect crystal oscillator drives the clock, the clock skew $dC_i(t)/dt - 1 = \rho_i(t)$ is not constant, particularly during warm-up [19]. We therefore define

$$C_i(t) = t + \Theta_i(t), \quad (10)$$

where $\Theta_i(t) = C_i(t) - t$ is the offset of the module's local clock to real time. It is calculated to be

$$\Theta_i(t) = \Theta_i(t_0) + \int_{t_0}^{t} \rho_i(\tau) d\tau, \quad (11)$$

where $\Theta_i(t_0)$ is the offset at time t_0 and where the skew $\rho_i(t)$ is assumed to be a random walk process driven by zero-mean noise $w_{\rho'}$ [20]:

$$\rho_i'(t) = w_{\rho'}(t). \quad (12)$$

B. Clock Synchronization Protocol

The anchors' clocks must be synchronized in order to allow transmission timestamps to be compared. To synchronize the anchor clocks, the time interval between a signal being transmitted from anchor 0, and being received at anchor i must be known. This timespan $\zeta_{0,i}$ is

$$\zeta_{0,i} = \Delta^0 + f_{0,i} + \Delta^i \quad (13)$$

with $f_{0,i}$ the time of flight and Δ^0 and Δ^i the transmission and reception delay, respectively. It is measured using the two-way communication protocol presented in [6].

After each anchor i has measured $\zeta_{0,i}$, the anchors transition to using a one-way communication protocol. This protocol is shown in Fig. 4 and begins with anchor 0 sending two subsequent signals, delayed by $\delta_{\text{pulse pair}}$, containing their respective transmission times. Using the time-difference

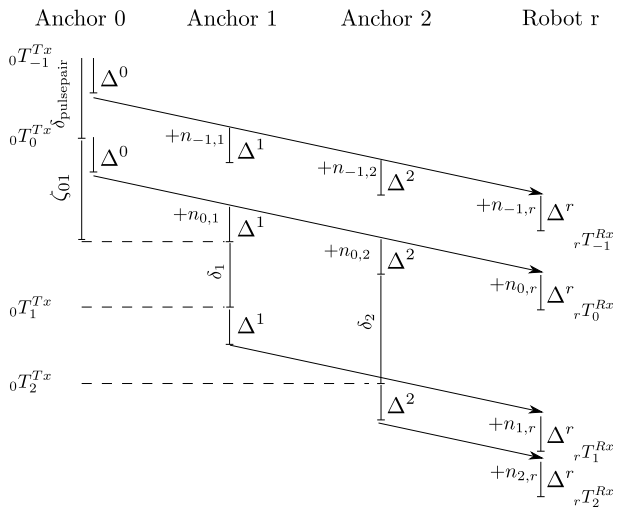

Fig. 4. The one-way communication protocol described in Subsection III-B with the transmission and reception timestamps T^{Tx}, T^{Rx} of the signals

between the arrival of these two messages, anchor i is able to calculate its relative skew to anchor 0 as

$$\rho_{0,i} = \frac{{}_0T_0^{Tx} - {}_0T_{-1}^{Tx}}{{}_iT_0^{Rx} - {}_iT_{-1}^{Rx}} - 1, \tag{14}$$

with ${}_iT_k^{Tx}$ the transmission time of signal k as expressed in the time of anchor i. Knowing $\zeta_{0,i}$ and $\rho_{0,i}$ anchor i can synchronize its clock to anchor 0.

After receiving the second signal from anchor 0, anchor i waits a predefined time δ_i after which its sends a signal containing the transmission timestamps expressed in the time of anchor 0. Once all anchors have sent such a signal, the one-way protocol is repeated.

This light-weight clock synchronization protocol enables TOA and TDOA measurements at a high frequency, however, does not scale to large anchor networks, since multihopping is not possible and as it relies on a reference anchor to synchronize the network. Synchronization protocols for larger networks are discussed, for example, in [13], [18].

C. Measurements

The one-way communication algorithm presented above enables the robot to localize itself using either TOA or TDOA measurements, assuming anchor positions are known.

The algorithm enables TOA measurements (1) to be calculated as

$$f_i = {}_rT_i^{Rx} - {}_0T_i^{Tx}, \tag{15}$$

and TDOA measurements (3) to be calculated as

$$d_{i,j} = (\rho_{0,r}+1)({}_rT_i^{Rx} - {}_rT_j^{Rx}) - ({}_0T_i^{Tx} - {}_0T_j^{Tx}). \tag{16}$$

Note that inherent in the reception timestamps ${}_rT_i^{Rx}$ and ${}_rT_j^{Rx}$ are measurement and transmission noise terms n_i and n_j.

IV. Evaluation

To evaluate the performance of the anchor algorithm presented in Section III for localization in two dimensions, measurements generated using the system were compared with ground-truth measurements from a motion-capture system and post-processed.

A. Setup

The anchor algorithm was implemented in C++ on STM32F4DiscoveryBoards, which served as host microcontrollers to the Decawave DWM1000 UWB modules. The motion capture system in the Flying Machine Arena [21] provided the ground truth for these measurements, providing position measurements with sub-centimeter accuracy at a frequency of 200 Hz.

Anchor 0 was programmed to send two subsequent signals delayed by $\delta_{\text{pulse pair}} = 1\,\text{ms}$ every 10 ms. All the other anchors delayed their signal by $\delta_i = i\,\text{ms}$, hence a complete set of TOA or TDOA measurements was obtained every 10 ms. Note that a minimum of two TDOA measurements or three TOA measurements with unknown clock offset are required for localization in two dimensions.

B. Measurement Quality

Measurements were gathered while orbiting anchor 1 as shown in Fig. 3 and Fig. 5. The upper plot of Fig. 6 shows TDOA measurement errors. It can be seen that although the error variance remains constant across azimuth angle ϕ, the mean of the TDOA error is angle dependent. Given line-of-sight conditions present during the experiment, this dependence on measurement angle is most likely caused by the radiation pattern of the UWB antennas, which is not isotropic [22]. The resulting varying signal delays cause biased measurements [19]. Additionally, the combined error

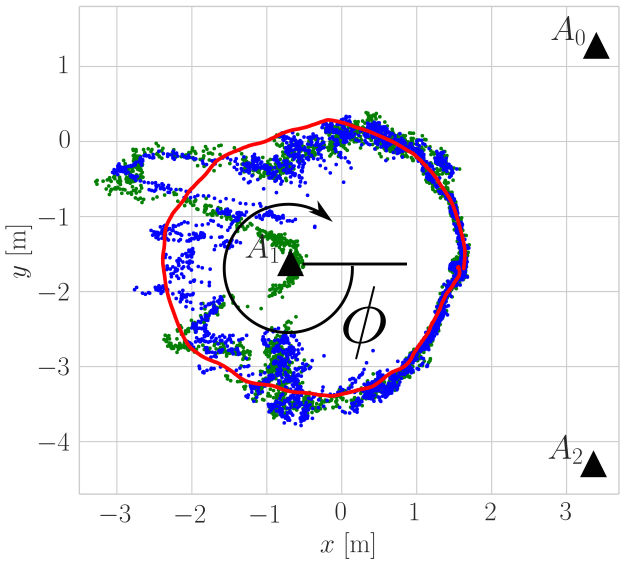

Fig. 5. This figure shows the position estimates generated by an EKF using TOA measurements (blue) and by an EKF using TDOA measurements (green). In both cases, a random-walk model was assumed.

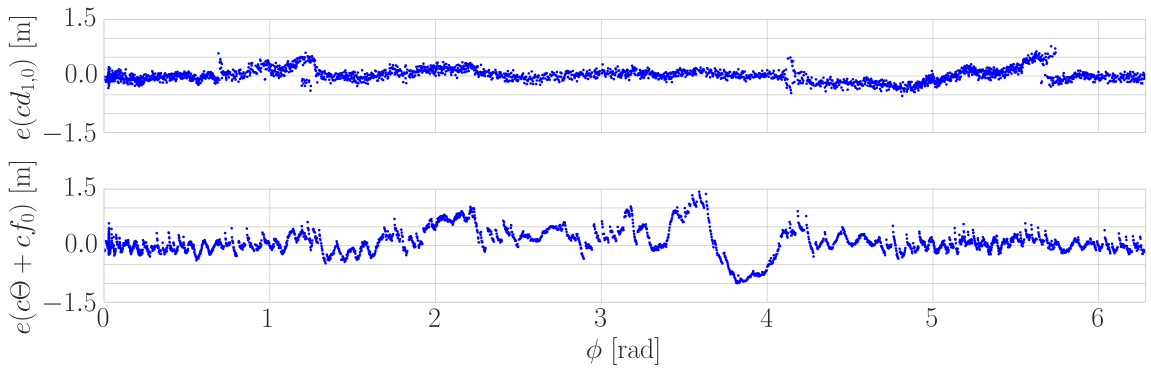

Fig. 6. Upper plot: TDOA measurement error between anchor 0 and anchor 1 ($e(cd_{1,0})$) for the setup shown in Fig. 3 and Fig. 5 for different values of ϕ. Lower plot: Combined error of clock estimate of the TOA EKF described in section IV-C and the TOA measurements of anchor 0 ($e(c\Theta + cf_0)$)

of the TOA measurements and the estimated clock offset of the filter discussed in the following subsection is shown in the lower plot of Fig. 6.

C. Random Walk TOA and TDOA Extended Kalman Filters

In order to verify whether these measurements are accurate enough for localization, measurement data was post-processed for both TOA and TDOA measurements, using an extended Kalman filter (EKF) and the assumption of a random-walk model for both position and clock skew. To be insensitive to modeling errors, the process noise on the position was assumed to be zero-mean noise $w_{x,y}$ with a large standard deviation of $\mathrm{SD}(\frac{w_{x,y}}{\Delta t}) = 20\,\mathrm{m\,s^{-1}}$ and the sampling time $\Delta t = 10\,\mathrm{ms}$. The standard deviation of the zero-mean driving noise on the skew w_ρ was set to be $\mathrm{SD}(\frac{w_\rho}{\Delta t}) = 0.1\,\mathrm{ppm/s}$. In normal operation this value is lower, however during warm-up the crystal oscillators show substantial drift [19].

In the case of TDOA measurements, clock offset was not tracked (since it does not appear in the measurement equation). Therefore, the system equations for the TDOA EKF are:

$$x(t+\Delta t) = x(t) + w_x(t) \tag{17}$$
$$y(t+\Delta t) = y(t) + w_y(t) \tag{18}$$
$$\rho(t+\Delta t) = \rho(t) + w_\rho(t). \tag{19}$$

In the case of TOA measurements, the EKF additionally includes clock offset Θ as a state, enabling clock synchronization. The system equations (17)-(19) are therefore extended by:

$$\Theta(t+\Delta t) = \Theta(t) + \rho(t)\Delta t. \tag{20}$$

The measurement equations for the TOA update are given by (1) and the one for the TDOA update by (3). Skew was measured directly using (14).

The noise n acting on the reception timestamps was assumed to have a standard deviation of $\sigma_f = 0.8\,\mathrm{ns}$. This value is an order of magnitude larger than expected ($\sigma_f = 0.06\,\mathrm{ns}$ [6]); however, this noise assumption was necessary due to the unmodeled measurement bias and imperfect clock synchronization. Both EKF were updated with a complete set of measurements to deal with the correlated noise of the TDOA measurements.

Fig. 5 shows the position estimates of the two filters. As expected, given the CRLB analysis in Section II, both filters perform well inside the convex hull of the anchors; however, as the robot leaves the convex hull, the position estimates deteriorates significantly, since the sensitivity to measurement errors is large. Since the TOA EKF additionally tracks the clock offset, it performs slightly better outside the convex hull. However, the performance is heavily dependent on the variance assumptions: if the process noise on the skew is insufficient to capture not only the measurement noise, but also the angle-dependent measurement bias (non-zero-mean measurement noise), both clock offset and position estimates can drift off for the TOA EKF as is visible in the lower plot of Fig. 6 and in Fig. 5 at $\phi \approx 3.9\,\mathrm{rad}$. In such cases, it is advantageous not to track the clock.

V. Quadrocopter Integration

In the previous section, post-processing of TOA and TDOA measurements showed good results inside the convex hull. To demonstrate that the localization system is also applicable to real-time, dynamic systems, it was integrated with a quadrocopter. TDOA measurements were provided to the quadrocopter's onboard state estimator. The TDOA approach was chosen since the quadrocopter flew only within the convex hull of the anchors (which differ in location from pervious experiments, as described in Subsection V-C). Clock skew was estimated independently.

A. Setup

The quadrocopter's onboard estimator is described in [6] and uses the accelerometer to update the airspeed estimate. It was adapted to use TDOA measurements by linearizing the TDOA measurement equation (3) around the quadrocopter's current state estimate. In addition to TDOA measurements, and the measurements required by the estimator [6], a barometer was used to reduce estimation variance in the

vertical direction. For the relation between the pressure p and the robot's altitude z, the isothermic barometric formula was used [23]:

$$p(z) = p(z_{\text{ref}}) \exp\left(-\frac{MG}{RT}(z - z_{\text{ref}})\right), \tag{21}$$

with $M = 28.97\,\text{g}\,\text{mol}^{-1}$ the molar mass of air, $G = 9.81\,\text{m}\,\text{s}^{-1}$ the gravitational acceleration, $R = 8.314\,\text{J}\,\text{mol}^{-1}\,\text{K}$ the universal gas constant for air, $T = 295\,\text{K}$ the absolute temperature of the air which is assumed constant, and z_{ref} the altitude at which the estimator was initialized.

This estimator was implemented in C++ and was run at 1000 Hz on a Pixhawk PX4 flight management unit [24]. In addition to the estimator and localization system, an onboard state controller was used to track a position setpoint, which was sent via a radio command from a ground station. This flight management unit and a DWM1000 module connected to it over SPI were mounted on a Hummingbird quadrocopter [25].

B. Estimator Settings

The parameters of the extended Kalman filter were left unchanged from the values described in [6], with the exception of the acceleration process noise, which was set to have a standard deviation of $5\,\text{m}\,\text{s}^{-2}$ because of the higher UWB update rate. In addition, the barometer measurement noise was set to have a standard deviation of 0.15 mbar which equals an altitude difference of about 1.3 m for ambient conditions.

To facilitate a smooth quadrocopter flight in the presence of biased TDOA measurements, their standard deviation was set to 3 m. This value was tuned by hand.

C. Experiment

The quadrocopter was commanded to fly a horizontal square ten times by moving the position setpoint with a speed of $1\,\text{m}\,\text{s}^{-1}$. The square had a length of 3.4 m and its center coincided with the center of the cuboid spanned by eight anchors with side-length $\Delta x \approx 9\,\text{m}$, $\Delta y \approx 5.5\,\text{m}$ and $\Delta z \approx 5\,\text{m}$ (see Table I for coordinates). This square is shown in Fig. 7 whereas the (x, y, z) position and the RMS error of the estimator are shown in Fig. 8.

D. Discussion and Interpretation

Fig. 7 shows the trajectory tracking for x and y position. Due to the proportional position control, the quadrocoptor lagged the setpoint and did not accurately track the square's vertices. Fig. 8 shows that the RMS error of the x and y position is significantly smaller than the RMS error of the overall position (when z is included). The former has a mean of 0.14 m, whereas the latter has a mean of 0.28 m. One explanation for the poor vertical tracking could be the anchor setup, which showed the least variance in the z positions of the anchors and only approximated the optimal anchor placement criteria outlined in [17]. Another possible cause could be the airspeed estimation in the thrust direction being more sensitive to errors.

TABLE I
ANCHOR COORDINATES FOR THE QUADROCOPTER MANEUVER

Nr.	0	1	2	3	4	5	6	7
x [m]	-4.3	4.0	-4.7	4.0	3.8	3.8	-5.8	-5.8
y [m]	-4.7	1.7	1.2	-4.2	-4.7	1.3	-2.2	1.5
z [m]	0.3	5	0.3	5	0.3	0.3	6.1	6.1

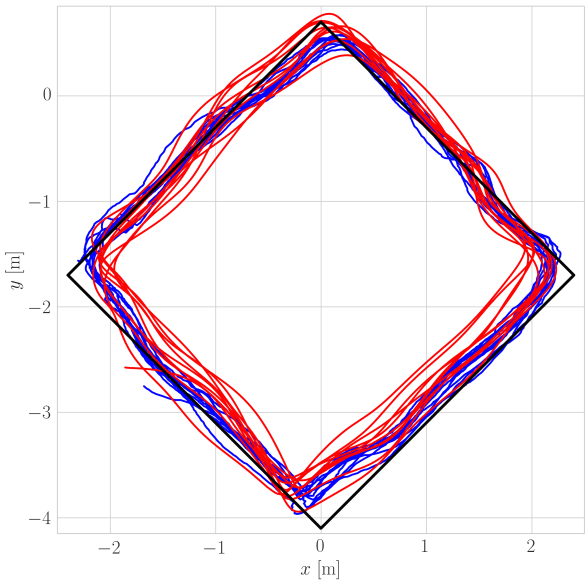

Fig. 7. The position setpoint for the quadrocopter was moved with $1\,\text{m}\,\text{s}^{-1}$ along the reference trajectory (black). The actual (red) and the estimated (blue) position of the quadrocopter are shown during this maneuverer. See Table I for the anchor coordinates.

VI. Conclusion

This paper presented a localization system that enables robot localization within some space. By receiving one-way communication from a set of fixed-position anchors, a robot is able to self-localize using either TOA or TDOA measurements. Since robots are not active in the communication process and are able to self-localize, the system supports multiple robots operating simultaneously and anonymously within the space.

In its current embodiment, the localization system is experimentally shown to perform well enough for a quadrocopter to repeatably track a reference trajectory over an extended period of time with a RMS error of 0.28 m. However, experimental results show that systematic measurement biases exist and vary throughout the space. Since these biases are location-dependent, unknown and thus not compensated for in the state estimation, they cause noticeable degradation in localization performance, biasing TOA measurements by up to 0.3 m. A non-isotropic antenna radiation pattern is hypothesized to be the cause of these biases.

In addition to systematic errors, the TDOA measurement standard deviation was 0.075 m – larger than the expected

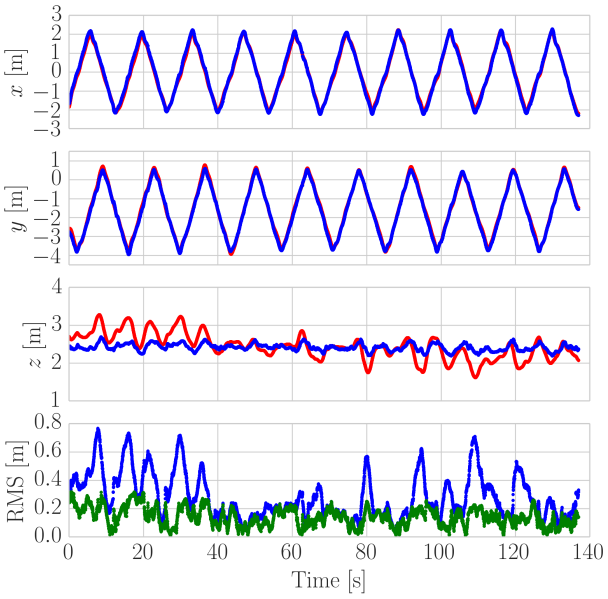

Fig. 8. The actual (red) and estimated (blue) (x,y,z) position during the quadrocopter maneuver. Lowest plot: In blue, the RMS error between estimated $(\hat{x},\hat{y},\hat{z})$ position and actual (x,y,z) position. In green the RMS error between the estimated $(\hat{x},\hat{y})$ position and the actual (x,y) position. This plot shows that the localization system accurately estimates position in the xy-plane (with a mean horizontal position RMS error: 0.14 m), but less well when the vertical direction is also considered (with a mean position RMS error: 0.28 m).

$c\sqrt{2}\sigma_f = 0.025\,\text{m}$. This is most likely due to imperfect anchor clock synchronization. It is suggested that alternative algorithms for clock synchronization be investigated in order to reduce this variance.

With the low computational cost of onboard self-localization, the good scalability and the high update frequency, this system appears to be suited to investigate swarm robotics or to serve as a cheap and flexible alternative to motion capture systems if sub-decimeter position accuracy is not required.

Acknowledgments

The authors would like to thank Mark W. Mueller for his advice concerning integration with the quadrocopter system. Aspects of this paper were only possible due to the work of numerous collaborators in the Flying Machine Arena project [21].

References

[1] N. Samama, *Global positioning : technologies and performance*, ser. Wiley survival guides in engineering and science. Hoboken, NJ: Wiley-Interscience, 2008.

[2] J.-A. Fernndez-Madrigal and J. L. Blanco Claraco, *Simultaneous localization and mapping for mobile robots : introduction and methods*, ser. Premier reference source. Hershey, PA: Information Science Reference, 2013.

[3] M. Field, D. Stirling, F. Naghdy, and Z. Pan, "Motion capture in robotics review," in *IEEE International Conference on Control and Automation (ICCA)*, Dec. 2009, pp. 1697–1702.

[4] H. Liu, H. Darabi, P. Banerjee, and J. Liu, "Survey of Wireless Indoor Positioning Techniques and Systems," *IEEE Transactions on Systems, Man, and Cybernetics, Part C: Applications and Reviews*, vol. 37, no. 6, pp. 1067–1080, Nov. 2007.

[5] J. L. Rullan-Lara, G. Sanahuja, R. Lozano, S. Salazar, R. Garcia-Hernandez, and J. A. Ruz-Hernandez, "Indoor Localization of a Quadrotor Based on WSN: A Real-Time Application," *International Journal of Advanced Robotic Systems*, 2013.

[6] M. W. Mueller, M. Hamer, and R. D'Andrea, "Fusing ultra-wideband range measurements with accelerometers and rate gyroscopes for quadrocopter state estimation," in *IEEE International Conference on Robotics and Automation (ICRA)*, May 2015, pp. 1730–1736.

[7] R. Dalce, A. van den Bossche, and T. Val, "Indoor self-localization in a WSN, based on Time Of Flight: Propositions and demonstrator," in *International Conference on Indoor Positioning and Indoor Navigation (IPIN)*, Oct. 2013.

[8] S. Krishnan, P. Sharma, Z. Guoping, and O. H. Woon, "A UWB based Localization System for Indoor Robot Navigation," in *IEEE International Conference on Ultra-Wideband (ICUWB)*, Sep. 2007, pp. 77–82.

[9] Y. K. Cho, J. H. Youn, and D. Martinez, "Error modeling for an untethered ultra-wideband system for construction indoor asset tracking," *Automation in Construction*, vol. 19, no. 1, pp. 43–54, Jan. 2010.

[10] R. Fontana, E. Richley, and J. Barney, "Commercialization of an ultra wideband precision asset location system," in *IEEE Conference on Ultra Wideband Systems and Technologies*, Nov. 2003, pp. 369–373.

[11] A. Prorok and A. Martinoli, "Accurate indoor localization with ultra-wideband using spatial models and collaboration," *The International Journal of Robotics Research*, vol. 33, no. 4, pp. 547–568, Apr. 2014.

[12] K. Yu, I. Sharp, and Y. J. Guo, *Ground-based wireless positioning*, ser. IEEE Press series on digital & mobile communication. Chichester, West Sussex, UK: Wiley, 2009.

[13] M. Y. M. Mah, "Time-based Location Techniques Using Inexpensive, Unsynchronized Clocks in Wireless Networks," 2011. [Online]. Available: http://drum.lib.umd.edu/handle/1903/11695

[14] M. Frederik Michel Dekking, *A modern introduction to probability and statistics : understanding why and how*, ser. Springer texts in statistics. London: Springer, 2005.

[15] R. Kaune, "Accuracy studies for TDOA and TOA localization," in *15th International Conference on Information Fusion (FUSION)*, Jul. 2012, pp. 408–415.

[16] T. Sathyan, M. Hedley, and M. Mallick, "An analysis of the error characteristics of two time of arrival localization techniques," in *13th Conference on Information Fusion (FUSION)*, Jul. 2010, pp. 1–7.

[17] J. T. Isaacs, D. J. Klein, and J. P. Hespanha, "Optimal sensor placement for time difference of arrival localization," in *IEEE Conference on Decision and Control (CDC)*. IEEE, Dec. 2009, pp. 7878–7884.

[18] B. Sundararaman, U. Buy, and A. D. Kshemkalyani, "Clock synchronization for wireless sensor networks: A Survey," *Ad Hoc Networks (Elsevier*, vol. 3, pp. 281–323, 2005.

[19] "APS011 Application Note Sources of Error in DW1000 Based Two-Way Ranging (TWR) Schemes," 2014. [Online]. Available: http://www.decawave.com/sites/default/files/resources/aps011_sources_of_error_in_twr.pdf

[20] Y. Bar-Shalom, X.-R. Li, and T. Kirubarajan, *Estimation with applications to tracking and navigation*. New York: Wiley-Interscience, 2001.

[21] S. Lupashin, M. Hehn, M. W. Mueller, A. P. Schoellig, M. Sherback, and R. DAndrea, "A platform for aerial robotics research and demonstration: The Flying Machine Arena," *Mechatronics*, vol. 24, no. 1, pp. 41–54, Feb. 2014.

[22] "DWM1000 Datasheet," 2014. [Online]. Available: http://www.decawave.com/sites/default/files/resources/dwm1000-datasheet-v1.01.pdf

[23] C. Johannes Karl Fink, *Physical chemistry in depth*. Berlin: Springer, 2009.

[24] L. Meier, P. Tanskanen, L. Heng, G. H. Lee, F. Fraundorfer, and M. Pollefeys, "PIXHAWK: A micro aerial vehicle design for autonomous flight using onboard computer vision," *Autonomous Robots*, vol. 33, no. 1-2, pp. 21–39, Feb. 2012.

[25] D. Gurdan, J. Stumpf, M. Achtelik, K.-M. Doth, G. Hirzinger, and D. Rus, "Energy-efficient Autonomous Four-rotor Flying Robot Controlled at 1 kHz," in *2007 IEEE International Conference on Robotics and Automation*, Apr. 2007, pp. 361–366.